Regioselective Derivatization of Silylated [20]Silafulleranes

Marcel Bamberg,[†] Thomas Gasevic,[‡] Michael Bolte,[†] Alexander Virovets,[†] Hans-Wolfram Lerner,[†] Stefan Grimme, [‡] Markus Bursch,[§,*] Matthias Wagner[†,*]

[†]Institut für Anorganische und Analytische Chemie, Goethe-Universität Frankfurt am Main, Max-von-Laue-Straße 7, 60438 Frankfurt am Main (Germany)

[‡]Mulliken Center for Theoretical Chemistry, Clausius-Institut für Physikalische und Theoretische Chemie, Rheinische Friedrich-Wilhelms-Universität Bonn, Beringstraße 4, 53115 Bonn (Germany)

[§]Max-Planck-Institut für Kohlenforschung, Kaiser-Wilhelm-Platz 1, 45470 Mülheim an der Ruhr (Germany)

ABSTRACT: Silafulleranes with endohedral Cl^- ions are a unique, scarcely explored class of structurally well-defined silicon clusters and host-guest complexes. Herein, we report regioselective derivatization reactions on the siladodecahedrane [*n*Bu$_4$N][Cl@Si$_{20}$(SiCl$_3$)$_{12}$Cl$_8$] ([*n*Bu$_4$N][**1**]), which has its cluster surface decorated with 12 $SiCl_3$ and 8 Cl substituents in perfect T_h symmetry. Room-temperature reaction of [*n*Bu$_4$N][**1**] with excess *i*Bu$_2$AlH in *ortho*-difluorobenzene (*o*DFB) furnishes perhydrogenated [*n*Bu$_4$N][Cl@Si$_{20}$(SiH$_3$)$_{12}$H$_8$] ([*n*Bu$_4$N][**2**]) in 50% yield; the non-pyrophoric [**2**]$^-$ is the largest structurally authenticated (by XRD) hydridosilane known to-date. A simple switch from pure *o*DFB to an *o*DFB/Et$_2$O solvent mixture suppresses core hydrogenation and results in the formation of [*n*Bu$_4$N][Cl@Si$_{20}$(SiH$_3$)$_{12}$Cl$_8$] ([*n*Bu$_4$N][**3**]). In addition to the exhaustive Cl/H exchange at all 44 Si–Cl bonds of [**1**]$^-$ and the regioselective 36-fold silyl-group hydrogenation, we achieved the simultaneous introduction of Me substituents at all 8 SiCl vertices along with the conversion of all 12 $SiCl_3$ to SiH_3 groups by treating [*n*Bu$_4$N][**1**] with Me$_2$AlH/Me$_3$Al in *o*DFB ([*n*Bu$_4$N][Cl@Si$_{20}$(SiH$_3$)$_{12}$Me$_8$], [*n*Bu$_4$N][**4**]; 73%). Quantum-chemical free-energy calculations find an S_N2-Si type hydrogenation of the exohedral $SiCl_3$ moieties in [**1**]$^-$ (trigonal-bipyramidal intermediate) slightly preferred over metathesis-like S_Ni-Si substitutions (four-membered transition state). Cage hydrogenation can occur only via S_Ni-Si processes. The experimentally demonstrated influence of an Et$_2$O co-solvent, which drastically increases the respective reaction barriers, is attributed to the increased stability of the resulting *i*Bu$_2$AlH-OEt$_2$ adduct and its higher steric bulk compared to free *i*Bu$_2$AlH.

INTRODUCTION

The discovery of the siladodecahedrane [*n*Bu$_4$N][Cl@Si$_{20}$(SiCl$_3$)$_{12}$Cl$_8$] ([*n*Bu$_4$N][**1**]; Figure 1) in 2015 provided the first preparative access to the class of compounds known as silafulleranes,[1] which had already received much attention from the theoretical chemistry community.[2–5] [*n*Bu$_4$N][**1**] is straightforwardly available from Si$_2$Cl$_6$, [*n*Bu$_4$N]Cl, and *n*Bu$_3$N in one step and in about 30% yield.[1,6] The anion [**1**]$^-$ consists of a dodecahedral Si$_{20}$ core carrying 12 $SiCl_3$ groups and 8 Cl atoms in a perfectly T_h-symmetric pattern and hosting a Cl^- ion as endohedral guest. This Cl^- ion likely plays a crucial role as a structure-directing template during the assembly of the silafullerane cluster before it is eventually encapsulated into it. Furthermore, it imparts a negative charge to the cluster, which facilitates the isolation of the salt-like product by crystallization and its analysis by LDI mass spectrometry in the negative-ion mode.[1] The presence of Si–Cl bonds in the substituent sphere of [**1**]$^-$ is uncommon in the field of molecular Si and Ge clusters,[7] since most of the saturated clusters reported so far, such as tetrasilatetrahedranes,[8,9] octasilacubanes,[10,11] or decasilaadamantane[12,13] and its isomers,[12,14] are decorated with rather inert alkyl, aryl, or organosilyl groups. Nevertheless, various routes of derivatization have been developed, including reductive[9] or nucleophilic[13] removal of substituents, oxidative cage opening,[15,16] and one-electron reduction of the cluster core.[17] Furthermore, a rich chemistry of unsaturated, so-called "metalloid"[18] Si and Ge clusters[19–24] and completely ligand-free Zintl ions has evolved.[25–31]

Coming back to the silafullerane [*n*Bu$_4$N][**1**], its follow-up chemistry can be developed along two paths (Figure 1): 1) stripping of the 12 $SiCl_3$ groups to enter the area of Si$_{20}$ clusters and 2) derivatization of [**1**]$^-$ while preserving its Si$_{32}$ framework. Following path 1, our groups have recently synthesized and characterized the parent siladodecahedrane with endohedral Cl^- ion, [Cl@Si$_{20}$H$_{20}$]$^-$ (Figure 1),[32] and put an end to previous, exclusively theory-based, discussions on the existence of the I_h-symmetric Si$_{20}$H$_{20}$ cage.[3,5] Our synthesis builds upon the protodesilylation of [**1**]$^-$ with pinacol and a subsequent Cl/H exchange on the primary product [Cl@Si$_{20}$H$_{12}$Cl$_8$]$^-$ with diisobutylaluminium hydride (*i*Bu$_2$AlH). Perchlorination of [Cl@Si$_{20}$H$_{20}$]$^-$ to afford [Cl@Si$_{20}$Cl$_{20}$]$^-$ was achieved by treatment with chloromethanes. Due to their highly symmetric environments in the centers of the silafulleranes [**1**]$^-$, [Cl@Si$_{20}$H$_{12}$Cl$_8$]$^-$, [Cl@Si$_{20}$H$_{20}$]$^-$, and [Cl@Si$_{20}$Cl$_{20}$]$^-$, the en-

dohedral Cl^- ions give rise to unusually sharp ^{35}Cl NMR signals and observable J(H,Cl) and J(Si,Cl) couplings in the respective NMR spectra. After a thorough quantum-chemical analysis of the shielding components, we found that the chemical shift value $\delta(^{35}Cl)$ provides a useful analytical probe for evaluating the degree of endohedral $Cl^-\rightarrow Si_{20}$ charge transfer.[32]

Herein, we are now focusing on path 2 (Scheme 1a) and disclose (i) the perhydrogenation of [**1**]$^-$ to furnish $[Cl@Si_{20}(SiH_3)_{12}H_8]^-$ ([**2**]$^-$), (ii) a regioselective partial Cl/H exchange on [**1**]$^-$ to give $[Cl@Si_{20}(SiH_3)_{12}Cl_8]^-$ ([**3**]$^-$), and (iii) a regioselective three-component reaction to afford $[Cl@Si_{20}(SiH_3)_{12}Me_8]^-$ ([**4**]$^-$). The new syntheses are complemented by theoretical studies of the underlying reaction mechanisms, the importance of which goes far beyond our specific cluster chemistry, as they improve the understanding of chlorosilane hydrogenation in general.

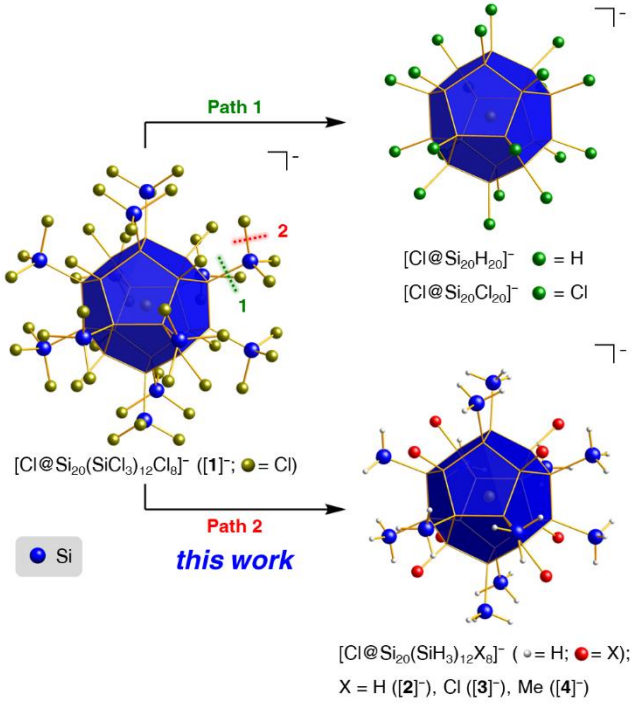

Figure 1. Fundamental approaches to the derivatization of [**1**]$^-$ (paths 1 and 2). Path 1: Desilylation allowing the synthesis of Si_{20} dodecahedranes. Path 2: Derivatization preserving the original Si_{32} framework.

RESULTS AND DISCUSSION

Hydridosilanes, along with halosilanes and organosilanes, are among the most versatile classes of silicon compounds, but examples of large, non-polymeric representatives are still rare.[33,34] The same is true for selectively mixed-substituted oligosilanes. The synthesis of hydrogenated silafullerenes with molecular weights of around 1000 g mol^{-1} is therefore an important objective to get access to the largest structurally well-defined hydridosilanes known to date. The high degree of functionalization of [**1**]$^-$ is both a blessing and a calamity. To cope with this ambivalent situation, we set out to develop not only reactions that allow quantitative derivatization of all 44 Si–Cl bonds ([**2**]$^-$), but also protocols that enable substitution of a specific number of Cl atoms by either functional groups of orthogonal reactivity ([**3**]$^-$) or by inert substituents ([**4**]$^-$).

Syntheses. In a previous report, we have already disclosed that [**2**]$^-$ was formed from [nBu$_4$N][**1**] and Li[AlH$_4$] in small amounts, which were, however, sufficient to detect [**2**]$^-$ by ^{29}Si and $^1H^{29}Si$-HMBC NMR spectroscopy as well as LDI mass spectrometry.[1] This protocol suffers from a partial degradation of the silafullerane with concomitant formation of pyrophoric SiH_4, a known problem in the hydrogenation of chlorinated oligosilanes:[33,35] Li[AlH$_4$] appears to be nucleophilic enough to cleave not only Si–Cl-, but also Si–Si bonds. Moreover, the Li[AlX$_4$] (X = H, Cl) byproducts are tedious to remove and therefore impede the purification of [nBu$_4$N][**2**]. We now report that both obstacles can be overcome by using excess diisobutylaluminium hydride (iBu$_2$AlH; 100 equiv) as a Lewis-acidic and neutral H$^-$ source that substitutes all 44 exohedral Cl atoms of [nBu$_4$N][**1**] with H atoms in the non-donor solvent *ortho*-difluorobenzene (*o*DFB; Scheme 1a). In this way, non-pyrophoric [nBu$_4$N][**2**] was obtained in a typical yield of 50% and in the form of single crystals suitable for X-ray crystallography. The compound is significantly less soluble in *o*DFB than [nBu$_4$N][**1**], but is relatively well soluble in THF without undergoing decomposition. The suitability of *o*DFB for reactions with [nBu$_4$N][**1**] is particularly noteworthy: due to its combination of high dipole moment, non-basicity, high stability towards Lewis acids, and moderate boiling point,[36] it became the solvent of choice for all subsequent transformations.

We next explored the possibility of selectively replacing only the 36 Cl atoms on the sterically exposed $SiCl_3$ groups of [**1**]$^-$ with H atoms to generate the silafullerane [nBu$_4$N][**3**]. An initial reaction of [nBu$_4$N][**1**] with 36 equiv of iBu$_2$AlH in *o*DFB again gave solely crystals of [nBu$_4$N][**2**]. The selective synthesis of [nBu$_4$N][**3**] was finally achieved by simply switching from pure *o*DFB as the solvent to an equimolar mixture of *o*DFB and Et$_2$O. After precipitation by addition of *n*-hexane and subsequent filtration, [nBu$_4$N][**3**] was isolated as a colorless powder in 40% yield. During the optimization of the synthesis protocol, we obtained X-ray-quality crystals of [nBu$_4$N][$Cl@Si_{20}(SiH_3)_{12}HCl_7$] ([$nBu_4$N][**3'**]; cf. the Supporting Information for details). In this compound, one of the 8 cluster-bonded Cl atoms is replaced by an H atom. As long as single crystals of [nBu$_4$N][**3**] are not available, the structure analysis of [nBu$_4$N][**3'**] will serve as a substitute to discuss the main geometric parameters of mixed H/Cl-silafulleranes.

The synthesis protocol for [nBu$_4$N][**4**] was inspired by a serendipitous discovery: Intending to replace iBu$_2$AlH with a more easily removable aluminium hydride in the synthesis of [nBu$_4$N][**2**], we treated [nBu$_4$N][**1**] with excess Me$_2$AlH. Indeed, we observed the desired quantitative Cl/H exchange at the 12 silyl groups of [**1**]$^-$; at its 8 SiCl moieties, however, not only Cl/H, but also Cl/Me exchange took place without a clear preference. This reaction can be developed into an efficient route to [nBu$_4$N][**4**] if more Me groups are supplied by using 44 equiv of Me$_2$AlH along with 30 equiv of Me$_3$Al. The product readily crystallizes from the *o*DFB/toluene solvent mixture in 73% yield.[37,38]

Scheme 1. (a) Syntheses of [*n*Bu$_4$N][2]–[*n*Bu$_4$N][4], starting from [*n*Bu$_4$N][1]. (b) Test reactions to shed light on the substituent-exchange mechanisms. (c) Crystallographically determined structures of the silafullerane salts [Et$_4$N][1],[1] [*n*Bu$_4$N][2], [*n*Bu$_4$N][3'], and [*n*Bu$_4$N][4] in the solid state (cations are omitted for clarity; in the structure of [3']$^-$, H and Cl are equally disordered over the two sites marked with red asterisks).

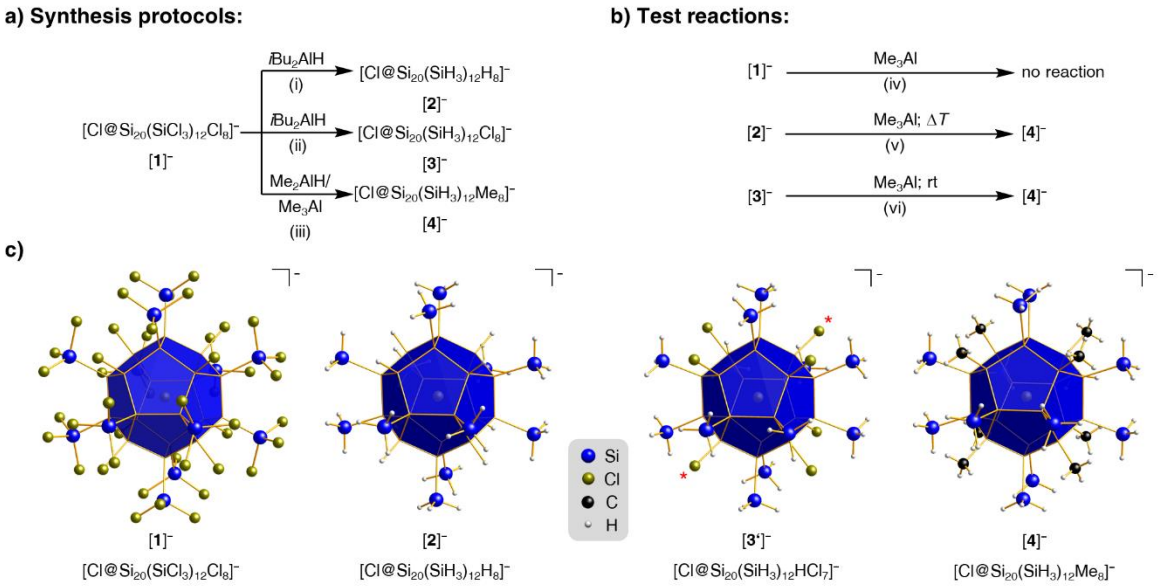

Reagents and conditions: (i) 100 equiv *i*Bu$_2$AlH, *o*DFB, rt, 1 d. Yield: 50%; (ii) 40 equiv *i*Bu$_2$AlH, *o*DFB/Et$_2$O (1:1), rt, 18 h. Yield: 40%. (iii) 44 equiv Me$_2$AlH, 30 equiv Me$_3$Al, *o*DFB/toluene, rt, 3 d. Yield: 73%. (iv) 120 equiv Me$_3$Al, *o*DFB/toluene, rt, 1 d. (v) 80 equiv Me$_3$Al, *o*DFB/toluene, 100 °C, 21 h. (vi) 80 equiv Me$_3$Al, *o*DFB/toluene, rt, <1 h.

Having optimized the synthesis of [*n*Bu$_4$N][**4**], we subsequently performed several test reactions to shed some light on critical aspects of the underlying three-component reaction. The following results were obtained (Scheme 1b): 1) [*n*Bu$_4$N][**1**] is inert toward Me$_3$Al in the absence of Me$_2$AlH (room temperature). 2) [*n*Bu$_4$N][**2**] undergoes eightfold H/Me exchange at its core when treated with Me$_3$Al in the absence of Me$_2$AlH (100 °C).[39] 3) [*n*Bu$_4$N][**3**] undergoes eightfold Cl/Me exchange at its core when treated with Me$_3$Al in the absence of Me$_2$AlH (room temperature). From these results, the following picture emerges: The aluminium hydride not only serves as H$^-$ source for the silyl groups, but also helps to activate the system for Me transfer to the cluster core. A direct mode of action would be the formation of reactive (Me$_2$AlH)$_x$(Me$_3$Al)$_y$ aggregates. A more indirect influence could be primarily based on the initial conversion of SiCl$_3$ to SiH$_3$, because (i) pre-coordination of Me$_3$Al to a silyl-H atom would render Me transfer an intramolecular reaction,[40] and (ii) the lower steric demand and group electronegativity of SiH$_3$ vs. SiCl$_3$ should facilitate Cl$^-$ abstraction from the Si$_{20}$ core. Moreover, the higher temperature required for reaction 2) as opposed to 3) indicates that core methylation most likely occurs at Si–Cl rather than intermediately formed Si–H bonds. It is probably not a "self-healing" process that corrects "false" core hydrogenation.

To validate the experimental findings and to gain deeper insight into the SiCl$_3$ vs. core-SiCl hydrogenation mechanisms, quantum-chemical calculations were conducted. Theoretical considerations regarding the three-component reaction for regioselective hydrogenation/methylation are not discussed as the nature of the actual active H/Me-transfer reagent(s) is unknown and the number and sizes of potential candidates are prohibitively high.

Quantum-chemical calculations on the Cl/H-exchange mechanisms. Free energy calculations were performed at the r^{2}SCAN0-D4[41–43]/ma-def2-QZVPP[44,45]+COSMO-RS(CH$_2$Cl$_2$)[46,47]+G(mRRHO)[48,49]//PBEh-3c[50](SMD(CH$_2$Cl$_2$))[51] level using the xtb 6.5.1,[52,53] ORCA 5.0.3[54–56] and TURBOMOLE 7.6.0[57] program packages (cf. the Supporting Information for further details). To keep the computational effort within reasonable limits, we studied substitution reactions at the exohedral SiCl$_3$ groups and at the SiCl cluster vertices by using the model systems [**M1**]$^-$ and [**M2**]$^-$, respectively (Figure 2).

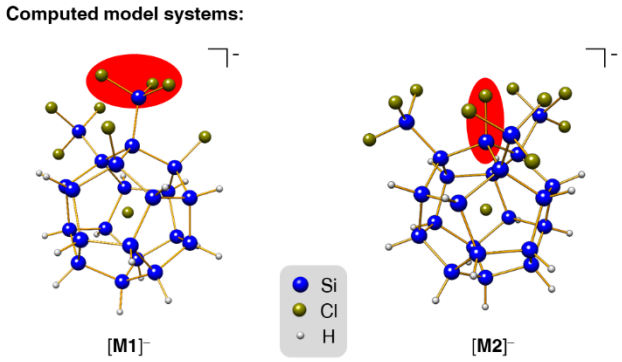

Figure 2. Model systems used for the computational studies of substitution reactions at the exohedral SiCl$_3$ groups ([**M1**]$^-$) and at the SiCl cluster vertices ([**M2**]$^-$). The functional groups under investigation are highlighted in red.

In [**M1**]⁻/[**M2**]⁻, we consider one Si–$SiCl_3$/Si–Cl moiety and treat only their three adjacent vertices explicitly, while the rest of the cluster is simplified to 16 Si–H vertices.

Two possible mechanisms for the hydrogenation of chlorosilanes using *i*Bu_2AlH are known in the literature.[58-61] In Scheme 2, these are illustrated by the example of an exohedral $SiCl_3$ group of [**1**]⁻: The so-called "intramolecular nucleophilic substitution mechanism" (S_Ni-Si) involves a four-membered transition state, whereas the S_N2-Si mechanism includes a trigonal-bipyramidal structure. The latter resembles the transition state of an S_N2 reaction at a carbon center but is a true intermediate because the silicon atom can become hypercoordinated.

Scheme 2. Hydrogenation following the S_Ni-Si or S_N2-Si mechanism at an exohedral $SiCl_3$ group.

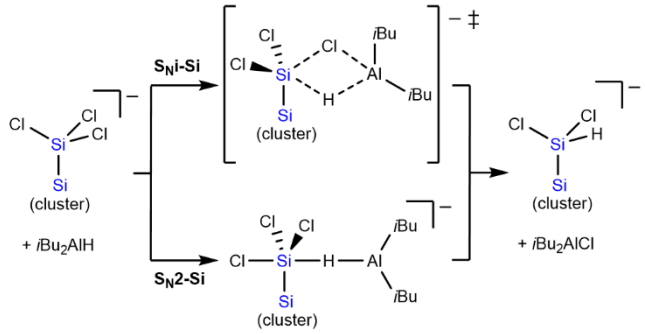

Since the potential energy curves around these intermediates are very shallow, S_N2-Si transition states connecting them with reactants and products could not be located. However, exactly because the energy differences between the transition states and the intermediates must be small in the present cases, we can use the intermediates' energies to gain insight into the favored reaction mechanisms even without knowledge of the transition states. While the S_Ni-Si mechanism is geometrically possible at both the $SiCl_3$ and SiCl functionalities, S_N2-Si hydrogenation can only take place at $SiCl_3$ because the backside attack at SiCl is blocked by the cluster core.[62] A comparison of the S_Ni-Si barrier heights already reveals that the barrier for SiCl hydrogenation is almost twice as large as that for $SiCl_3$ hydrogenation ($\Delta G^‡$(TS2) = 21.4 kcal mol⁻¹, $\Delta G^‡$(TS4) = 11.5 kcal mol⁻¹ $\Delta\Delta G^‡$ = 9.9 kcal mol⁻¹; Figure 3). The free-energy difference $\Delta\Delta G^‡$ for Cl/H exchange at the two positions increases even to 12.4 kcal mol⁻¹, if we take into account that S_N2-Si hydrogenation at $SiCl_3$ is slightly more favorable than S_Ni-Si hydrogenation (cf. ΔG(INT5) = 9.0 kcal mol⁻¹ vs. $\Delta G^‡$(TS4) = 11.5 kcal mol⁻¹): in the S_N2 intermediate, *i*Bu_2AlH is precoordinated to the neighboring SiCl vertex and is therefore already in close vicinity to the reacting $SiCl_3$ group. Most importantly, the barrier height for SiCl hydrogenation decreases from $\Delta G^‡$(TS2) = 21.4 to $\Delta G^‡$(TS2.1) = 17.6 kcal mol⁻¹ once the $SiCl_3$ groups are fully hydrogenated, which explains why the cluster core is also eventually perhydrogenated to afford [**2**]⁻. Addition of Et_2O to the reaction mixture leads to the formation of an *i*Bu_2AlH-OEt_2 adduct, which not only increases the steric demand of the hydrogenation reagent, but also stabilizes the adduct by 16.6 kcal mol⁻¹ compared to free *i*Bu_2AlH. As a result, both the $SiCl_3$ and the SiCl hydrogenation are now associated with a higher energy penalty (ΔG(INT3) = 17.3 kcal mol⁻¹, $\Delta G^‡$(TS1) = 34.1 kcal mol⁻¹, $\Delta\Delta G^‡$ = 16.8 kcal mol⁻¹), but the $\Delta\Delta G^‡$ value further increases by 4.4 kcal mol⁻¹. While INT3 is still accessible at room temperature, TS1 lies energetically too high to be overcome under these conditions. Even after the exhaustive conversion of $SiCl_3$ to SiH_3, hydrogenation at the SiCl vertices still has a barrier of $\Delta G^‡$(TS1.1) = 32.8 kcal mol⁻¹, so that this reaction is largely suppressed at room temperature. Taken together, this explains why our synthesis protocol gives essentially pure samples of [**3**]⁻ with very little contamination from singly core-hydrogenated [**3'**]⁻ (Scheme 1c).

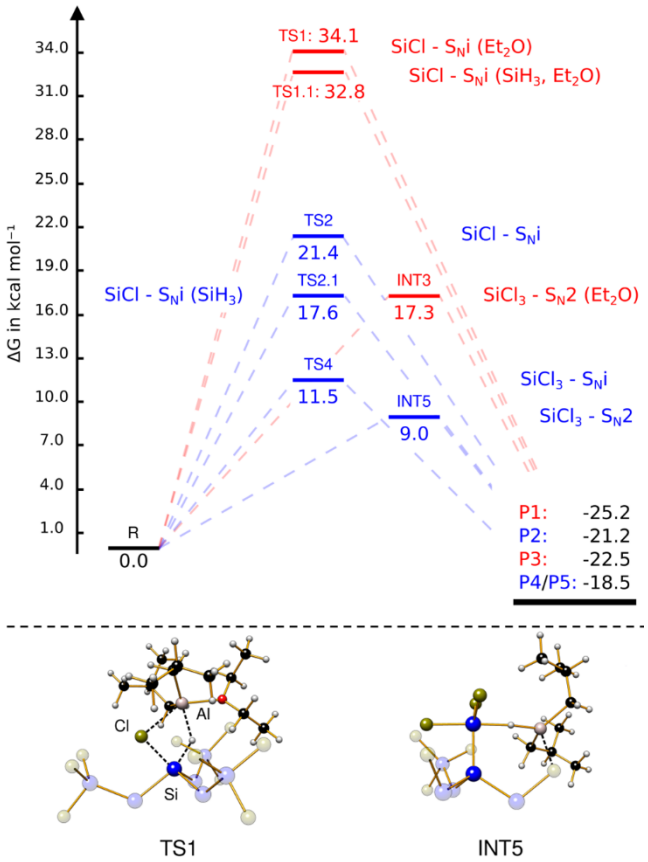

Figure 3. Calculated Gibbs free energies ΔG for the hydrogenation at the r²SCAN0-D4/ma-def2-QZVPP+COSMO-RS(CH_2Cl_2)+G(mRRHO)//PBEh-3c(SMD(CH_2Cl_2)) level of theory. R represents the separated reactants which are [**M1**]⁻ or [**M2**]⁻ in combination with the respective nucleophile. P represents the products obtained after a single hydrogenation step via the transition state or intermediate with the same number.

X-ray Crystal Structure Analyses, IR Spectroscopy, and LDI Mass Spectrometry. Scheme 1c shows the anion structures of [*n*Bu_4N][**2**], [*n*Bu_4N][**3'**], and [*n*Bu_4N][**4**] in the solid state (the structure of the known [**1**]⁻ was added for completeness). The proposed substitution patterns are fully confirmed. Careful analysis of the residual electron density in the regions near the SiMe and SiH_3 groups of [**4**]⁻ (based on high-quality diffraction data obtained with synchrotron radiation) provides no evidence for a possible Me/H crystallographic disorder. All anions lie on inversion centers; Si–H/Cl disorder in [**3'**]⁻ occurs only at two equivalent positions (marked with red asterisks). The Si–Si bond lengths of the three anions fall in the range 2.3200(5)–

2.381(6) Å.[63] For an assessment of the different propensities of differently substituted SiR cluster vertices to accept charge density from the endohedral Cl^- ion, the $Cl^-\cdots Si$ distances within each individual cluster are particularly diagnostic (Figure 4a; blue bars: range of experimental values, red lines: computed values). For $[\mathbf{2}]^-$, the ranges of $Cl\cdots SiH$ and $Cl\cdots SiSiH_3$ distances are overlapping. For $[\mathbf{3'}]^-$ and $[\mathbf{4}]^-$, the $Cl\cdots SiCl$[64] and $Cl\cdots SiMe$ distances are shorter and longer, respectively, than the corresponding $Cl\cdots SiSiH_3$ distances within the same molecule. This ordering fits to the expected trend in the acceptor-orbital energies according to σ*(Si–Me) > σ*(Si–SiH_3) ≈ σ*(Si–H) > σ*(Si–Cl).

In the solid-state IR spectra, bands at $\tilde{\nu}$(Si–H) = 2118 cm^{-1} ([*n*Bu_4N][**2**]; calcd 2160 cm^{-1}), 2138 cm^{-1} ([*n*Bu_4N][**3**]; calcd 2181 cm^{-1}), and 2102 cm^{-1} ([*n*Bu_4N][**4**]; calcd 2149 cm^{-1}) are assigned to the Si–H stretching modes of the SiH_3 groups. Only in the case of [*n*Bu_4N][**2**], additional, less intense Si–H stretching bands, originating from the SiH vertices, were detected ($\tilde{\nu}$(Si–H) = 2042 cm^{-1} and 2026 cm^{-1}, calcd 2101 cm^{-1}; cf. [*n*Bu_4N][Cl@$Si_{20}H_{20}$]:[32] $\tilde{\nu}$(Si–H) = 2064 cm^{-1}). Since IR wavenumbers correlate directly with the force constants and these, in turn, with the *s* character of the respective bonds, the experimentally observed trend in the H_2Si–H stretching modes indicates an increase in the *s* character in the order $[\mathbf{4}]^- < [\mathbf{2}]^- < [\mathbf{3}]^-$ (Figure 4b). This claim is further supported by a comparison of the corresponding ^1J(Si,H) NMR coupling constants, which also grow larger along the sequence $[\mathbf{4}]^- < [\mathbf{2}]^- < [\mathbf{3}]^-$, thereby testifying to an increasing Fermi contact interaction. Theoretical validation comes from Bent's rule[65] and a DFT-based natural localized molecular orbital (NLMO) analysis conducted with the NBO 6.0 program,[66,67] which predicts Si(*s*)-orbital contributions to the H_2Si–H bonds of 23.6% < 23.9% < 25.3%.

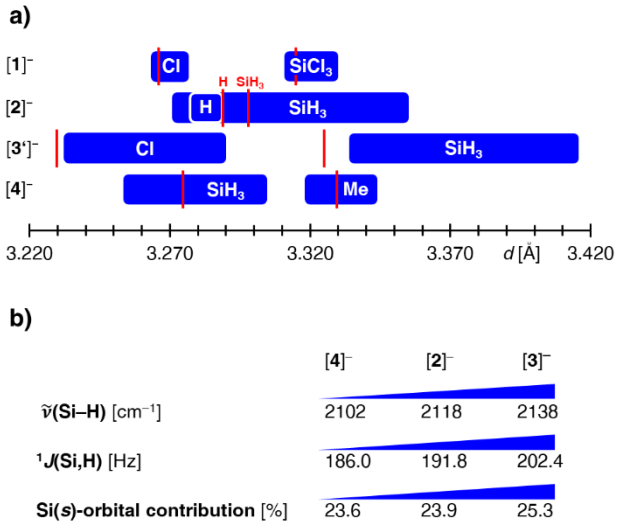

Figure 4. (a) Distances Cl···SiR between the endohedral Cl^- ions and the vertices of the Si_{20} cages in $[\mathbf{1}]^-$, $[\mathbf{2}]^-$, $[\mathbf{3'}]^-$, and $[\mathbf{4}]^-$ (blue bars: experimental ranges within 3σ margins, white font: specification of R; red lines: computed values). (b) Correlations between the experimentally obtained stretching frequencies ($\tilde{\nu}$(Si–H)) and NMR coupling constants (^1J(Si,H)) with the computed Si(*s*)-orbital contribution to the H_2Si–H bonds in $[\mathbf{4}]^-$, $[\mathbf{2}]^-$, and $[\mathbf{3}]^-$.

Laser-desorption ionization (LDI) MS(–) measurements on [*n*Bu_4N][**2**]–[*n*Bu_4N][**4**] gave the molecular-ion peaks $[M]^-$ of $[\mathbf{2}]^-$–$[\mathbf{4}]^-$ with fitting isotope patterns. Similar to $[\mathbf{1}]^-$, which undergoes gas-phase elimination of $SiCl_2$ units under LDI-MS conditions,[1] we now see evidence of SiH_2 elimination/insertion (-/+ 30 Da).

NMR Spectroscopy. The NMR spectra of [*n*Bu_4N][**2**] and [*n*Bu_4N][**4**] were recorded in THF-d_8, whereas [*n*Bu_4N][**3**] had to be characterized in *o*DFB/C_6D_{12} (5:1 mixture) due to its lability to donor solvents. The SiH_3 and Si*H* moieties of [*n*Bu_4N][**2**] give rise to a singlet at 3.47 ppm (36H) and a 1:1:1:1 quartet at 4.31 ppm (8H; J(H,Cl) = 2.9 Hz), respectively. Upon ^{35}Cl decoupling, the quartet collapses into a singlet with broadened base (due to unresolved coupling to ^{37}Cl; $S(^{35}Cl) = S(^{37}Cl) = 3/2$, natural abundances: 75.5% and 24.5%[68]).[69] The exclusively peripheral hydrogenation in $[\mathbf{3}]^-$ is evident from the absence of core-SiH resonances. The complete core methylation in $[\mathbf{4}]^-$ is reflected by the SiH_3 vs. core-SiMe integral ratio of 36H vs. 24H.

In its ^{29}Si{^{1}H} NMR spectrum, each of the T_h-symmetric silafulleranes $[\mathbf{2}]^-$–$[\mathbf{4}]^-$ shows three resonances for the chemically inequivalent Si^0, Si^I, and Si^{III} centers. The corresponding chemical shifts agree well with the computed values (Table 1).[70,71]

Table 1. Experimental (calculated) ^{29}Si and ^{35}Cl NMR-spectroscopic parameters of the silafulleranes [*n*Bu_4N][1]–[*n*Bu_4N][4].[a] Calculated NMR shifts have been computed at the PBE0[72](COSMO(CH_2Cl_2))[73]/SO-ZORA/TZP[74] level of theory.

Compound	$\delta(^{29}Si)$			$\delta(^{35}Cl)$
	Si^0	Si^I	Si^{III}	
[*n*Bu_4N][**1**]	–60.3	31.1	10.3	274.5
	(–63.5)	(31.7)	(15.9)	(277.6)[b]
[*n*Bu_4N][**2**]	–58.5	–14.9	–93.7	469.0
	(–58.3)	(–23.9)	(–98.6)	(471.8)[b]
[*n*Bu_4N][**3**]	–73.4	51.5	–97.7	363.7
	(–72.6)	(54.3)	(–98.5)	(360.0)[b]
[*n*Bu_4N][**4**]	–67.2	19.1	–100.6	457.1
	(–67.3)	(21.3)	(–102.4)	(455.8)[b]

[a] NMR spectra were recorded in THF-d_8 ([*n*Bu_4N][**1**],[1,7] [*n*Bu_4N][**2**], [*n*Bu_4N][**4**]) or *o*DFB/C_6D_{12} (5:1; [*n*Bu_4N][**3**]). [b] These values were obtained after scaling according to the following linear equation: $\delta(^{35}Cl, \text{scaled}) = 0.8739 \cdot \delta(^{35}Cl, \text{calcd}) - 8.3536$.

The endohedral Cl^- ions within the highly symmetric siladodecahedrane cages of $[Cl@Si_{20}R_{20}]^-$ (R = H, Cl) give rise to sharp ^{35}Cl resonances.[32] Based on a quantum-chemical analysis of the shielding components, we have shown that $\delta(^{35}Cl)$ is a useful probe of the degree of the $Cl^- \rightarrow Si_{20}$ host-guest interaction: a downfield shift of the ^{35}Cl signal is diagnostic for a decreased $Cl^- \rightarrow Si_{20}$ charge transfer, as illustrated by a comparison of $[Cl@Si_{20}Cl_{20}]^-$ (126.0 ppm; more electronegative substituents) and $[Cl@Si_{20}H_{20}]^-$ (345.0 ppm; less electronegative substituents).[32] In line with that, the presence of even less electronegative SiH_3 substituents[75] in $[\mathbf{2}]^-$ is accompanied by a further down-

field shift to $\delta(^{35}Cl)$ = 469.0 (Table 1; cf. also [**4**]$^-$). $\delta(^{35}Cl)$ = 363.7 of the partly chlorinated [**3**]$^-$ lies between the shifts of [**2**]$^-$ and exhaustively chlorinated [**1**]$^-$ (274.5 ppm).[32] Our measured $\delta(^{35}Cl)$ values were verified by spin–orbit relativistic DFT calculations,[72–74,76–79] which gave an excellent fit after scaling according to the following linear equation: $\delta(^{35}Cl, scaled) = 0.8739 \cdot \delta(^{35}Cl, calcd) - 8.3536$ (cf. the Supporting Information for more details).

As discussed above, our early attempts at the synthesis of [*n*Bu$_4$N][**4**] from [*n*Bu$_4$N][**1**] and Me$_2$AlH (without Me$_3$Al) resulted in a product mixture. In the $^{35}Cl\{^1H\}$ NMR spectrum, this mixture gave rise to a multitude of resonances in the range 469.1–456.8 ppm. Since the two range limits fit to the shift values of [*n*Bu$_4$N][**2**] (8 core-SiH) and [*n*Bu$_4$N][**4**] (8 core-SiMe; Table 1), it is reasonable to assume that the resonances in between belong to mixed-substituted silafulleranes [*n* core-SiH + (8–*n*) core-SiMe; *n* = 1–7]. On the other hand, this conclusion is at odds with previous experience gained from [Cl@Si$_{20}$(H/Cl)$_{20}$]$^-$ silafulleranes, where any symmetry breaking had resulted in such severely broadened ^{35}Cl signals that they were no longer detectable. One possible solution of this riddle would be that unsymmetrically distributed core-SiH/SiMe leads to a smaller electric field gradient (EFG) than unsymmetrically distributed core-SiH/SiCl. A smaller EFG should accelerate the relaxation of the ^{35}Cl quadrupole nucleus to a lesser extent, resulting in a narrower resonance line.

The influence of the substitution pattern on the EFG within a silafullerane cage was investigated by DFT calculations on selected derivatives. To a good approximation, the NMR line width $\Delta\nu$ is proportional to the square of the largest principal component of the EFG tensor, V_{33}^2 (cf. the Supporting Information for more details).[80–82] For T_h-symmetric [Cl@Si$_{20}$H$_{12}$Cl$_8$]$^-$ and [**4**]$^-$, the computed V_{33}^2 values for the endohedral Cl$^-$ ion are close to 0[83] (compare the exohedral Cl substituents of [Cl@Si$_{20}$H$_{12}$Cl$_8$]$^-$ with V_{33}^2 = 4.44 a.u.). For the less symmetric isomer of [Cl@Si$_{20}$H$_{12}$Cl$_8$]$^-$, in which one H and one Cl atom have changed places, and for [Cl@Si$_{20}$H$_{11}$Cl$_9$]$^-$, in which one H atom is replaced by one Cl atom, V_{33}^2 increases to values in the order of 1×10^{-2} a.u. In stark contrast, hundredfold smaller values $V_{33}^2 \leq 1\times10^{-4}$ a.u. were computed for an isomer of [**4**]$^-$, in which one cage-bonded Me group and one silyl-bonded H atom have changed places, and for [Cl@Si$_{20}$(SiH$_3$)$_{12}$HMe$_7$]$^-$, in which one cage-bonded Me group is replaced by one H atom. Therefore, it should indeed be more likely to detect ^{35}Cl NMR signals of [**4**]$^-$-type than of [Cl@Si$_{20}$H$_{12}$Cl$_8$]$^-$-type compounds with slight deviations from the perfect T_h-symmetric substitution pattern.

CONCLUSION

Starting from the perchlorinated silafullerane [*n*Bu$_4$N][Cl@Si$_{20}$(SiCl$_3$)$_{12}$Cl$_8$], we developed facile synthesis routes to the perhydrogenated [*n*Bu$_4$N][Cl@Si$_{20}$(SiH$_3$)$_{12}$H$_8$] ([*n*Bu$_4$N][**2**]; *i*Bu$_2$AlH in *o*DFB), the partially hydrogenated [*n*Bu$_4$N][Cl@Si$_{20}$(SiH$_3$)$_{12}$Cl$_8$] ([*n*Bu$_4$N][**3**]; *i*Bu$_2$AlH in *o*DFB/Et$_2$O), and the regioselectively mixed-substituted [*n*Bu$_4$N][Cl@Si$_{20}$(SiH$_3$)$_{12}$Me$_8$] ([*n*Bu$_4$N][**4**]; Me$_2$AlH/Me$_3$Al in *o*DFB/toluene, *o*DFB = *ortho*-difluorobenzene). According to quantum-chemical calculations, SiCl$_3$ hydrogenation (via an S_N2-Si-type scenario) is kinetically more favorable than core-SiCl hydrogenation (via an S_Ni-Si-type transition state). This explains why taming the reactivity of *i*Bu$_2$AlH through Et$_2$O-adduct formation suppresses core hydrogenation and ultimately furnishes [**3**]$^-$ instead of [**2**]$^-$. Experimentally obtained structural and spectroscopic parameters of [**2**]$^-$–[**4**]$^-$ are in very good agreement with computed values. A theoretical assessment of the electric field gradients (EFGs) experienced by the encapsulated Cl$^-$ ions of selected silafulleranes helps to understand why the corresponding ^{35}Cl resonances of [**4**]$^-$-type compounds are detectable even if the strict T_h symmetry is violated, whereas these signals are broadened beyond detection in comparable symmetry-broken H/Cl-mixed silafulleranes.

As an outlook, the Si–H bonds of [**2**]$^-$–[**4**]$^-$ are valuable functional groups for subsequent hydrosilylation[84,85] or dehydrogenative Si–Si coupling reactions.[86,87] Resulting silafullerane oligomers would be nano-sized compounds bridging the gap between small-molecule silanes and extended silicon-based solids.[88–91]

ASSOCIATED CONTENT

The Supporting Information is available free of charge at http://pubs.acs.org.
Experimental and computational details, as well as characterization data (PDF)
Cartesian coordinates of computed molecular structures (ZIP)
X-ray crystallographic data (CIF)

AUTHOR INFORMATION

Corresponding Authors

Matthias Wagner – *Institut für Anorganische und Analytische Chemie, Goethe-Universität Frankfurt am Main, 60438 Frankfurt am Main, Germany;* orcid.org/0000-0001-5806-8276; Email: matthias.wagner@chemie.uni-frankfurt.de
Markus Bursch – *Max-Planck-Institut für Kohlenforschung, 45470 Mülheim an der Ruhr, Germany;* orcid.org/0000-0001-6711-5804; Email: bursch@kofo.mpg.de

Authors

Marcel Bamberg – *Institut für Anorganische und Analytische Chemie, Goethe-Universität Frankfurt am Main, 60438 Frankfurt am Main, Germany*; orcid.org/0000-0001-6044-5077
Thomas Gasevic – *Mulliken Center for Theoretical Chemistry, Clausius-Institut für Physikalische und Theoretische Chemie, Rheinische Friedrich-Wilhelms-Universität Bonn, 53115 Bonn, Germany*; orcid.org/0000-0003-4864-1758
Michael Bolte – *Institut für Anorganische und Analytische Chemie, Goethe-Universität Frankfurt am Main, 60438 Frankfurt am Main, Germany*
Alexander Virovets – *Institut für Anorganische und Analytische Chemie, Goethe-Universität Frankfurt am Main, 60438 Frankfurt am Main, Germany*; orcid.org/0000-0002-8843-8503
Hans-Wolfram Lerner – *Institut für Anorganische und Analytische Chemie, Goethe-Universität Frankfurt am Main, 60438 Frankfurt am Main, Germany*; orcid.org/0000-0003-1803-7947

Stefan Grimme – *Mulliken Center for Theoretical Chemistry, Clausius-Institut für Physikalische und Theoretische Chemie, Rheinische Friedrich-Wilhelms-Universität Bonn, 53115 Bonn, Germany*; orcid.org/0000-0002-5844-4371

Funding Sources

M.W. thanks the Deutsche Forschungsgemeinschaft for financial support (DFG grant no. 506550642). S.G. and M.Bu. gratefully acknowledge financial support by the Max Planck Society through the Max Planck fellow program. M.Ba. wishes to thank the Fonds der Chemischen Industrie (FCI) for a Kekulé Ph.D. grant.

Notes

The authors declare no competing financial interests.

ACKNOWLEDGMENT

S.G., M.Bu., and T.G. thank Christoph Plett for fruitful discussions. The authors are grateful to Evonik Operations GmbH, Rheinfelden (Germany), for the generous donation of Si_2Cl_6. Parts of this research (project I-20220865) were carried out at PETRA III at DESY, a member of the Helmholtz Association (HGF). A.V. and M.Ba. thank Dr. Leila Noohinejad, Dr. Martin Tolkiehn and Dr. Eugenia Peresypkina for their assistance regarding the use of the beamline P24. A.V. thanks Dr. Matthias Meyer (Rigaku Oxford Diffraction) for his precious help with the implementation of the *CrysAlisPro* software for the synchrotron and STOE IPDS II diffraction data. M.Ba. wishes to thank Julius Wicke for preparative support.

REFERENCES

(1) Tillmann, J.; Wender, J. H.; Bahr, U.; Bolte, M.; Lerner, H.-W.; Holthausen, M. C.; Wagner, M. One-Step Synthesis of a [20]Silafullerane with an Endohedral Chloride Ion. *Angew. Chem., Int. Ed.* **2015**, *54*, 5429–5433. https://doi.org/10.1002/anie.201412050

(2) Nagase, S. Polyhedral Compounds of the Heavier Group 14 Elements: Silicon, Germanium, Tin, and Lead. *Acc. Chem. Res.* **1995**, *28*, 469–476. https://doi.org/10.1021/ar00059a005

(3) Pichierri, F.; Kumar, V.; Kawazoe, Y. Encapsulation of halide anions in perhydrogenated silicon fullerene: $X^-@Si_{20}H_{20}$ (X = F, Cl, Br, I). *Chem. Phys. Lett.* **2005**, *406*, 341–344. https://doi.org/10.1016/j.cplett.2005.02.121

(4) Marsusi, F.; Qasemnazhand, M. Sila-fulleranes: promising chemically active fullerene analogs. *Nanotechnology* **2016**, *27*, 275704. https://doi.org/10.1088/0957-4484/27/27/275704

(5) De, D. S.; Schaefer, B.; von Issendorff, B.; Goedecker, S. Nonexistence of the decahedral $Si_{20}H_{20}$ cage: Levinthal's paradox revisited. *Phys. Rev. B* **2020**, *101*, 214303. https://doi.org/10.1103/PhysRevB.101.214303

(6) Our group has developed the Si_2Cl_6/Cl^- system as a versatile trichlorosilylation reagent, which enables the synthesis of a wide range of silicon compounds such as Cl^--coordinated cyclohexasilanes, anionic organosilanes, germanides, and even mixed Si/Ge or Si/Sn heteroadamantanes: (a) Review: Teichmann, J.; Wagner, M. Silicon chemistry in zero to three dimensions: from dichlorosilylene to silafullerane. *Chem. Commun.* **2018**, *54*, 1397–1412. https://doi.org/10.1039/C7CC09063C (b) Tillmann, J.; Meyer, L.; Schweizer, J. I.; Bolte, M.; Lerner, H.-W.; Wagner, M.; Holthausen, M. C. Chloride-Induced Aufbau of Perchlorinated Cyclohexasilanes from Si_2Cl_6: A Mechanistic Scenario. *Chem. – Eur. J.* **2014**, *20*, 9234–9239. https://doi.org/10.1002/chem.201402655 (c) Köstler, B.; Bae, H.; Gilmer, J.; Virovets, A.; Lerner, H.-W.; Albert, P.; Fantuzzi, F.; Wagner, M. Dope it with germanium: selective access to functionalized Si_5Ge heterocycles. *Chem. Commun.* **2023**, *59*, 716–719. https://doi.org/10.1039/D2CC06060D (d) Georg, I.; Teichmann, J.; Bursch, M.; Tillmann, J.; Endeward, B.; Bolte, M.; Lerner, H.-W.; Grimme, S.; Wagner, M. Exhaustively Trichlorosilylated C_1 and C_2 Building Blocks: Beyond the Müller–Rochow Direct Process. *J. Am. Chem. Soc.* **2018**, *140*, 9696–9708. https://doi.org/10.1021/jacs.8b05950 (e) Georg, I.; Bursch, M.; Stückrath, J. B.; Alig, E.; Bolte, M.; Lerner, H.-W.; Grimme, S.; Wagner, M. Building up Strain in One Step: Synthesis of an Edge-Fused Double Silacyclobutene from an Extensively Trichlorosilylated Butadiene Dianion. *Angew. Chem., Int. Ed.* **2020**, *59*, 16181–16187. https://doi.org/10.1002/anie.202006463 (f) Georg, I.; Bursch, M.; Endeward, B.; Bolte, M.; Lerner, H.-W.; Grimme, S.; Wagner, M. The power of trichlorosilylation: isolable trisilylated allyl anions, allyl radicals, and allenyl anions. *Chem. Sci.* **2021**, *12*, 12419–12428. https://doi.org/10.1039/D1SC03958J (g) Teichmann, J.; Kunkel, C.; Georg, I.; Moxter, M.; Santowski, T.; Bolte, M.; Lerner, H.-W.; Bade, S.; Wagner, M. Tris(trichlorosilyl)tetrelide Anions and a Comparative Study of Their Donor Qualities. *Chem. – Eur. J.* **2019**, *25*, 2740–2744. https://doi.org/10.1002/chem.201806298 (h) Köstler, B.; Bolte, M.; Lerner, H.-W.; Wagner, M. Selective One-Pot Syntheses of Mixed Silicon-Germanium Heteroadamantane Clusters. *Chem. – Eur. J.* **2021**, *27*, 14401–14404. https://doi.org/10.1002/chem.202102732 (i) Köstler, B.; Gilmer, J.; Bolte, M.; Virovets, A.; Lerner, H.-W.; Albert, P.; Fantuzzi, F.; Wagner, M. Group IV heteroadamantanes: synthesis of Si_6Sn_4 and site-selective derivatization of Si_6Ge_4. *Chem. Commun.* **2023**, *59*, 2295–2298. https://doi.org/10.1039/D2CC06697A

(7) Heider, Y.; Scheschkewitz, D. Molecular Silicon Clusters. *Chem. Rev.* **2021**, *121*, 9674–9718. https://doi.org/10.1021/acs.chemrev.1c00052

(8) Wiberg, N.; Finger, C. M. M.; Polborn, K. Tetrakis(tri-*tert*-butylsilyl)-*tetrahedro*-tetrasilane (tBu$_3$Si)$_4$Si$_4$: The First Molecular Silicon Compound with a Si_4 Tetrahedron. *Angew. Chem., Int. Ed. Engl.* **1993**, *32*, 1054–1056. https://doi.org/10.1002/anie.199310541

(9) Ichinohe, M.; Toyoshima, M.; Kinjo, R.; Sekiguchi, A. Tetrasilatetrahedranide: A Silicon Cage Anion. *J. Am. Chem. Soc.* **2003**, *125*, 13328–13329. https://doi.org/10.1021/ja0305050

(10) Matsumoto, H.; Higuchi, K.; Hoshino, Y.; Koike, H.; Naoi, Y.; Nagai, Y. The First Octasilacubane System: Synthesis of Octakis-(t-butyldimethylsilyl)pentacyclo[4.2.0.0^{2,5}.0^{3,8}.0^{4,7}]-octasilane. *J. Chem. Soc., Chem. Commun.* **1988**, *3*, 1083–1084. https://doi.org/10.1039/C39880001083

(11) Furukawa, K.; Fujino, M.; Matsumoto, N. Cubic Silicon Cluster. *Appl. Phys. Lett.* **1992**, *60*, 2744–2745. https://doi.org/10.1063/1.106863

(12) Fischer, J.; Baumgartner, J.; Marschner, C. Synthesis and Structure of Sila-Adamantane. *Science* **2005**, *310*, 825. https://doi.org/10.1126/science.1118981

(13) Siu, T. C.; Imex Aguirre Cardenas, M.; Seo, J.; Boctor, K.; Shimono, M. G.; Tran, I. T.; Carta, V.; Su, T. A. Site-Selective Functionalization of Sila-Adamantane and Its Ensuing Optical Effects. *Angew. Chem., Int. Ed.* **2022**, *134*, e202206877. https://doi.org/10.1002/anie.202206877

(14) Tsurusaki, A.; Koyama, Y.; Kyushin, S. Decasilahexahydrotriquinacene and Decasilaisotwistane: σ Conjugation on a Bowl Surface. *J. Am. Chem. Soc.* **2017**, *139*, 3982–3985. https://doi.org/10.1021/jacs.7b00250

(15) Unno, M.; Higuchi, K.; Ida, M.; Shioyama, H.; Kyushin, S.; Matsumoto, H.; Goto, M. Ring-Opening Reaction of Octakis(1,1,2-trimethylpropyl)octasilacubane. Chlorination with PCl_5 Leading to Stereoisomeric 4,8-Dichlorooctakis(1,1,2-trimethylpropyl)-tetracyclo[3.3.0.0^{2,7}.0^{3,6}]octasilanes. *Organometallics* **1994**, *13*, 4633– 4640. https://doi.org/10.1021/om00023a075

(16) Wiberg, N.; Auer, H.; Nöth, H.; Knizek, J.; Polborn, K. Diiodotetrasupersilylcyclotetrasilene (tBu$_3$Si)$_4$Si$_4$I$_2$—A Molecule Containing an Unsaturated Si_4 Ring. *Angew. Chem., Int. Ed.* **1998**,

37, 2869–2872. https://doi.org/10.1002/(SICI)1521-3773(19981102)37:20<2869::AID-ANIE2869>3.0.CO;2-2

(17) Otsuka, K.; Matsumoto, N.; Ishida, S.; Kyushin, S. An Isolable Radical Anion of an Organosilicon Cluster Containing Only σ Bonds. *Angew. Chem., Int. Ed.* **2015**, *54*, 7833–7836. https://doi.org/10.1002/anie.201500523

(18) Schnepf, A.; Schnöckel, H. Metalloid Aluminum and Gallium Clusters: Element Modifications on the Molecular Scale? *Angew. Chem., Int. Ed.* **2002**, *41*, 3532–3554. https://doi.org/10.1002/1521-3773(20021004)41:19<3532::AID-ANIE3532>3.0.CO;2-4

(19) Scheschkewitz, D. A Molecular Silicon Cluster with a "Naked" Vertex Atom. *Angew. Chem., Int. Ed.* **2005**, *44*, 2954–2956. https://doi.org/10.1002/anie.200462730

(20) Heider, Y.; Poitiers, N. E.; Willmes, P.; Leszczyńska, K.; Huch, V.; Scheschkewitz, D. Site-selective functionalization of Si_6R_6 siliconoids. *Chem. Sci.* **2019**, *10*, 4523–4530. https://doi.org/10.1039/C8SC05591B

(21) Iwamoto, T.; Tsushima, D.; Kwon, E.; Ishida, S.; Isobe, H. Persilastaffanes: Design, Synthesis, Structure, and Conjugation between Silicon Cages. *Angew. Chem., Int. Ed.* **2012**, *51*, 2340–2344. https://doi.org/10.1002/anie.201106422

(22) Iwamoto, T.; Akasaka, N.; Ishida, S. A heavy analogue of the smallest bridgehead alkene stabilized by a base. *Nat. Commun.* **2014**, *5*, 5353. https://doi.org/10.1038/ncomms6353

(23) Keuter, J.; Schwedtmann, K.; Hepp, A.; Bergander, K.; Janka, O.; Doerenkamp, C.; Eckert, H.; Mück-Lichtenfeld, C.; Lips, F. Diradicaloid or Zwitterionic Character: The Non-Tetrahedral Unsaturated Compound $[Si_4\{N(SiMe_3)Dipp\}_4]$ with a Butterfly-Type Si_4 Substructure. *Angew. Chem., Int. Ed.* **2017**, *56*, 13866–13871. https://doi.org/10.1002/anie.201705787

(24) Keuter, J.; Schwermann, C.; Hepp, A.; Bergander, K.; Droste, J.; Hansen, M. R.; Doltsinis, N. L.; Mück-Lichtenfeld, C.; Lips, F. A highly unsaturated six-vertex amido-substituted silicon cluster. *Chem. Sci.* **2020**, *11*, 5895–5901. https://doi.org/10.1039/d0sc01427c

(25) Scharfe, S.; Kraus, F.; Stegmaier, S.; Schier, A.; Fässler, T. F. Zintl Ions, Cage Compounds, and Intermetalloid Clusters of Group 14 and Group 15 Elements. *Angew. Chem., Int. Ed.* **2011**, *50*, 3630–3670. https://doi.org/10.1002/anie.201001630

(26) Waibel, M.; Kraus, F.; Scharfe, S.; Wahl, B.; Fässler, T. F. $[(MesCu)_2(\eta^3\text{-}Si_4)]^{4-}$: A Mesitylcopper-Stabilized Tetrasilicide Tetraanion. *Angew. Chem., Int. Ed.* **2010**, *49*, 6611–6615. https://doi.org/10.1002/anie.201002153

(27) Schiegerl, L. J.; Karttunen, A. J.; Klein, W.; Fässler, T. F. Silicon clusters with six and seven unsubstituted vertices *via* a Two-Step Reaction from Elemental Silicon. *Chem. Sci.* **2019**, *10*, 9130–9139. https://doi.org/10.1039/C9SC03324F

(28) Goicoechea, J. M.; Sevov, S. C. $[(Ni\text{-}Ni\text{-}Ni)@(Ge_9)_2]^{4-}$: A Linear Triatomic Nickel Filament Enclosed in a Dimer of Nine-Atom Germanium Clusters. *Angew. Chem., Int. Ed.* **2005**, *44*, 4026–4028. https://doi.org/10.1002/anie.200500600

(29) Goicoechea, J. M.; Sevov, S. C. Deltahedral Germanium Clusters: Insertion of Transition-Metal Atoms and Addition of Organometallic Fragments. *J. Am. Chem. Soc.* **2006**, *128*, 4155–4161. https://doi.org/10.1021/ja058652g

(30) Joseph, S.; Hamberger, M.; Mutzbauer, F.; Härtl, O.; Meier, M.; Korber, N. Chemistry with Bare Silicon Clusters in Solution: A Transition-Metal Complex of a Polysilicide Anion. *Angew. Chem., Int. Ed.* **2009**, *48*, 8770–8772. https://doi.org/10.1002/anie.200904242

(31) Neumeier, M.; Fendt, F.; Gärtner, S.; Koch, C.; Gärtner, T.; Korber, N.; Gschwind, R. M. Detection of the Elusive Highly Charged Zintl Ions Si_4^{4-} and Sn_4^{4-} in Liquid Ammonia by NMR Spectroscopy. *Angew. Chem., Int. Ed.* **2013**, *52*, 4483–4486. https://doi.org/10.1002/anie.201209578

(32) Bamberg, M.; Bursch, M.; Hansen, A.; Brandl, M.; Sentis, G.; Kunze, L.; Bolte, M.; Lerner, H.-W.; Grimme, S.; Wagner, M. $[Cl@Si_{20}H_{20}]^-$: Parent Siladodecahedrane with Endohedral Chloride Ion. *J. Am. Chem. Soc.* **2021**, *143*, 10865–10871. https://doi.org/10.1021/jacs.1c05598

(33) Gerwig, M.; Böhme, U.; Friebel, M.; Gründler, F.; Franze, G.; Rosenkranz, M.; Schmidt, H.; Kroke, E. Syntheses and Molecular Structures of Liquid Pyrophoric Hydridosilanes. *ChemistryOpen* **2020**, *9*, 762–773. https://doi.org/10.1002/open.202000152

(34) For examples of structurally authenticated dendritic poly(methylsilane)s, see: (a) Lambert, J. B.; Wu, H. Synthesis and Crystal Structure of a Nanometer-Scale Dendritic Polysilane. *Organometallics* **1998**, *17*, 4904–4909. https://doi.org/10.1021/om980280f (b) Krempner, C.; Köckerling, M. Nanoscale Double-Core Oligosilane Dendrimers: Synthesis, Structure, and Electronic Properties. *Organometallics* **2008**, *27*, 346–352. https://doi.org/10.1021/om700544e

(35) Höfler, F.; Jannach, R. Zur Kenntnis des Neopentasilans. *Inorg. Nucl. Chem. Lett.* **1973**, *9*, 723–725. https://doi.org/10.1016/0020-1650(73)80226-0

(36) O'Toole, T. R.; Younathan, J. N.; Sullivan, B. P.; Meyer, T. J. 1,2-Difluorobenzene: A Relatively Inert and Noncoordinating Solvent for Electrochemical Studies on Transition-Metal Complexes. *Inorg. Chem.* **1989**, *28*, 3923–3926. https://doi.org/10.1021/ic00319a032

(37) Baldwin, S. M.; Bercaw, J. E.; Henling, L. M.; Day, M. W.; Brintzinger, H. H. Cationic Alkylaluminum-Complexed Zirconocene Hydrides: NMR-Spectroscopic Identification, Crystallographic Structure Determination, and Interconversion with Other Zirconocene Cations. *J. Am. Chem. Soc.* **2011**, *133*, 1805–1813. https://doi.org/10.1021/ja1050428

(38) Me_2AlH synthesized according to Ref. (37) necessarily requires a distillation step in the present case. Thereafter, ^1H NMR spectroscopy indicated a $Me_{2.2}AlH_{0.8}$ composition. For simplicity, we nevertheless refer to this compound as "Me_2AlH" throughout this paper but use the precise stoichiometry in the Supporting Information. In principle, Me_2AlH can be replaced with commercial *i*Bu_2AlH, but this leads to a slightly increased amount of side products.

(39) The corresponding reaction of [*n*Bu_4N][**2**] with the mixture Me_2AlH/Me_3Al again leads to core methylation; in the case of [*n*Bu_4N][**3**], the cluster is degraded.

(40) The isolable silane-alane complex $[Et_3Si–H\cdots Al(C_6F_5)_3]$ has been characterized by X-ray crystallography: Chen, J.; Chen, E. Y. X. Elusive Silane-Alane Complex [Si-H···Al]: Isolation, Characterization, and Multifaceted Frustrated Lewis Pair Type Catalysis. *Angew. Chem., Int. Ed.* **2015**, *54*, 6842–6846. https://doi.org/10.1002/anie.201502400. Furthermore, analogous Si–H···B interactions are essential for $B(C_6F_5)_3$-catalyzed hydrosilylation reactions and for the Piers-Rubinsztajn reaction: (a) Parks, D. J.; Piers, W. E. Tris(pentafluorophenyl)boron-Catalyzed Hydrosilation of Aromatic Aldehydes, Ketones, and Esters. *J. Am. Chem. Soc.* **1996**, *118*, 9440–9441. https://doi.org/10.1021/ja961536g (b) Brook, M. A. New Control Over Silicone Synthesis using SiH Chemistry: The Piers–Rubinsztajn Reaction. *Chem. – Eur. J.* **2018**, *24*, 8458–8469. https://doi.org/10.1002/chem.201800123

(41) Bursch, M.; Neugebauer, H.; Ehlert, S.; Grimme, S. Dispersion corrected r^2SCAN based global hybrid functionals: r^2SCANh, r^2SCAN0, and r^2SCAN50. *J. Chem. Phys.* **2022**, *156*, 134105. https://doi.org/10.1063/5.0086040

(42) Caldeweyher, E.; Bannwarth, C.; Grimme, S. Extension of the D3 dispersion coefficient model. *J. Chem. Phys.* **2017**, *147*, 034112. https://doi.org/10.1063/1.4993215

(43) Caldeweyher, E.; Ehlert, S.; Hansen, A.; Neugebauer, H.; Spicher, S.; Bannwarth, C.; Grimme, S. A generally applicable atomic-charge dependent London dispersion correction. *J. Chem. Phys.* **2019**, *150*, 154122. https://doi.org/10.1063/1.5090222

(44) Weigend, F.; Ahlrichs, R. Balanced basis sets of split valence, triple zeta valence and quadruple zeta valence quality for H to Rn: Design and assessment of accuracy. *Phys. Chem. Chem. Phys.* **2005**, *7*, 3297–3305. https://doi.org/10.1039/b508541a

(45) Zheng, J.; Xu, X.; Truhlar, D. G. Minimally augmented Karlsruhe basis sets. *Theor. Chem. Acc.* **2011**, *128*, 295–305. https://doi.org/10.1007/s00214-010-0846-z

(46) Klamt, A. Conductor-like Screening Model for Real Solvents: A New Approach to the Quantitative Calculation of Solvation Phenomena. *J. Phys. Chem.* **1995**, *99*, 2224–2235. https://doi.org/10.1021/j100007a062

(47) Klamt, A.; Jonas, V.; Bürger, T.; Lohrenz, J. C. W. Refinement and Parametrization of COSMO-RS. *J. Phys. Chem. A* **1998**, *102* (26), 5074–5085. https://doi.org/10.1021/jp980017s.

(48) Grimme, S. Supramolecular Binding Thermodynamics by Dispersion-Corrected Density Functional Theory. *Chem. – Eur. J.* **2012**, *18*, 9955–9964. https://doi.org/10.1002/chem.201200497

(49) Pracht, P.; Grimme, S. Calculation of absolute molecular entropies and heat capacities made simple. *Chem. Sci.* **2021**, *12*, 6551–6568. https://doi.org/10.1039/D1SC00621E

(50) Grimme, S.; Brandenburg, J. G.; Bannwarth, C.; Hansen, A. Consistent structures and interactions by density functional theory with small atomic orbital basis sets. *J. Chem. Phys.* **2015**, *143*, 054107. https://doi.org/10.1063/1.4927476

(51) Marenich, A. V.; Cramer, C. J.; Truhlar, D. G. Universal Solvation Model Based on Solute Electron Density and on a Continuum Model of the Solvent Defined by the Bulk Dielectric Constant and Atomic Surface Tensions. *J. Phys. Chem. B* **2009**, *113*, 6378–6396. https://doi.org/10.1021/jp810292n

(52) Bannwarth, C.; Caldeweyher, E.; Ehlert, S.; Hansen, A.; Pracht, P.; Seibert, J.; Spicher, S.; Grimme, S. Extended tight-binding quantum chemistry methods. *WIREs Comput. Mol. Sci.* **2021**, *11*, e1493. https://doi.org/10.1002/wcms.1493

(53) Grimme, S.; Bannwarth, C.; Shushkov, P. A Robust and Accurate Tight-Binding Quantum Chemical Method for Structures, Vibrational Frequencies, and Noncovalent Interactions of Large Molecular Systems Parametrized for All spd-Block Elements (*Z* = 1–86). *J. Chem. Theory Comput.* **2017**, *13*, 1989–2009. https://doi.org/10.1021/acs.jctc.7b00118

(54) Neese, F. The ORCA program system. *Wiley Interdiscip. Rev. Comput. Mol. Sci.* **2012**, *2*, 73–78. https://doi.org/10.1002/wcms.81

(55) Neese, F.; Wennmohs, F.; Becker, U.; Riplinger, C. The ORCA quantum chemistry program package. *J. Chem. Phys.* **2020**, *152*, 224108. https://doi.org/10.1063/5.0004608

(56) Neese, F. Software update: The ORCA program system—Version 5.0. *Wiley Interdiscip. Rev. Comput. Mol. Sci.* **2022**, *12*, e1606. https://doi.org/10.1002/WCMS.1606.

(57) TURBOMOLE V7.6 2021, a Development of Univesity of Karlsruhe and Forschungszentrum Karlsruhe GmbH, 1989-2007, TURBOMOLE GmbH, since 2007; available from http://www.turbomole.com (accessed 2023-04-21).

(58) Sommer, L. H.; McLick, J.; Golino, C. M. The S_Ni-Si Mechanism. Reductive Displacement of Good Leaving Groups with Retention of Configuration by Diisobutylaluminum Hydride. Stereochemical and Mechanistic Crossover with the Etherate Complex of Diisobutylaluminum Hydride. *J. Am. Chem. Soc.* **1972**, *94*, 669–670. https://doi.org/10.1021/ja00757a078

(59) Sommer, L. H.; Golino, C. M.; Roark, D. N.; Bush, R. D. Reduction of silicon halides and alkoxides with diisobutylaluminum hydride. Stereochemistry-rate law correlations for the *S_Ni-Si* and *S_N2-Si* mechanisms. *J. Organomet. Chem.* **1973**, *49*, C3–C5. https://doi.org/10.1016/S0022-328X(00)84916-5

(60) Corriu, R. J. P.; Guerin, C. Nucleophilic Displacement at Silicon: Recent Developments and Mechanistic Implications. *Adv. Organomet. Chem.* **1982**, *20*, 265–312. https://doi.org/10.1016/S0065-3055(08)60523-7

(61) Lainer, T.; Fischer, R.; Leypold, M.; Holthausen, M.; Wunnicke, O.; Haas, M.; Stueger, H. Unusually selective synthesis of chlorohydrooligosilanes. *Chem. Commun.* **2020**, *56*, 13812–13815. https://doi.org/10.1039/D0CC06506D

(62) Particularly in the present case, an S_N1-like mechanism for substituent exchange at the SiCl vertices would also be plausible, because the formal Si^+ center in the resulting neutral intermediate could be stabilized through interaction with the endohedral Cl^- ion. Our quantum-chemical calculations indicate that such a scenario is indeed reasonable from a thermodynamic point of view. Despite considerable efforts, however, we have not yet succeeded in modeling the entire reaction pathway, so that we are currently unable to draw definite conclusions regarding reaction kinetics.

(63) These values compare nicely to Si–Si = 2.339–2.393 Å within the fused Si_5 cycles of crystallographically characterized bicyclo[3.3.0]octasilanes: Kobayashi, H.; Iwamoto, T.; Kira, M. A Stable Fused Bicyclic Disilene as a Model for Silicon Surface. *J. Am. Chem. Soc.* **2005**, *127*, 15376–15377. https://doi.org/10.1021/ja055718z

(64) Only the 6 SiCl positions that are not affected by H/Cl disorder were considered.

(65) According to Bent's rule, the H_3Si group will direct a hybrid orbital with the highest *p* character toward the cluster with the highest group electronegativity. Since these group electronegativities follow the order [**4**]$^-$ < [**2**]$^-$ < [**3**]$^-$, the *p* character of the H_3Si–Si(cluster) bonds and, correspondingly, the *s* character of the H_2Si–H bonds should obey the same trend: Bent, H. A. An Appraisal of Valence-bond Structures and Hybridization in Compounds of the First-row Elements. *Chem. Rev.* **1961**, *61*, 275–311. https://doi.org/10.1021/cr60211a005

(66) Glendening, E. D.; Landis, C. R.; Weinhold, F. *NBO 6.0*: Natural bond orbital analysis program. *J. Comput. Chem.* **2013**, *34*, 1429–1437. https://doi.org/10.1002/jcc.23266

(67) Glendening, E. D.; Landis, C. R.; Weinhold, F. Erratum: NBO 6.0: Natural bond orbital analysis program. *J. Comput. Chem.* **2013**, *34*, 2134–2134. https://doi.org/10.1002/jcc.23366

(68) Akitt, J. W. The Quadrupolar Halides. In *Multinuclear NMR*; Mason, J., Ed.; Springer: Boston, 1987; pp 447–461. https://doi.org/10.1007/978-1-4613-1783-8_17

(69) Although *J*(H,Cl) coupling is only resolved for protons directly bonded to the Si_{20} core, we see a weak cross peak between the Si*H*$_3$ and ^{35}Cl resonances in the ^{1}H^{35}Cl-HMBC spectrum; a more intense cross peak appears between the Si*H* and ^{35}Cl resonances.

(70) As a characteristic NMR feature of our silafulleranes, the ^{29}Si nuclei of the cage vertices (Si^0/Si^I) are strongly deshielded relative to Si^0/Si^I centers of comparable open-chain oligosilanes; signals from Si^{III} in peripheral SiR_3 substituents of the same compound classes appear in the same region. Examples: (a) [*n*Bu$_4$N][**2**]: δ(^{29}Si) = –58.5 (Si^0), –14.9 (Si^I), –93.7 (Si^{III}); $HSi(SiH_3)_3$: δ(^{29}Si) = –137.4 (Si^I), –95.7 (Si^{III}); $Si(SiH_3)_4$: δ(^{29}Si) = –165.7 (Si^0), –90.4 (Si^{III}).[33] (b) [*n*Bu$_4$N][**1**]: δ(^{29}Si) = 31.1 (Si^I); [*n*Bu$_4$N][**3**]: δ(^{29}Si) = 51.5 (Si^I); $(Me_3Si)_3SiCl$: δ(^{29}Si) = –13.3 (Si^I);[92] [*n*Bu$_4$N][**2**]: δ(^{29}Si) = –14.9 (Si^I); $(Me_3Si)_3SiH$: δ(^{29}Si) = –115.4 (Si^I);[92] [*n*Bu$_4$N][**4**]: δ(^{29}Si) = 19.1 (Si^I); $(Me_3Si)_3SiMe$: δ(^{29}Si) = –87.9 (Si^I). For δ(^{29}Si) of $(Me_3Si)_3SiX$ (X = Cl, H, Me), see: Marsmann, H. C.; Raml, W.; Hengge, E. ^{29}Si-Kernresonanzmessungen an Polysilanen 2. Isotetrasilane. *Z. Naturforsch., B: Anorg. Chem., Org. Chem.* **1980**, *35*, 1541–1547. https://doi.org/10.1515/znb-1980-1211

(71) A previous theoretical study already suggested that the encapsulation of a Cl^- ion has a significant shielding effect on ^{29}Si nuclei of Si^I centers of $Si_{20}(SiCl_3)_{12}Cl_8$, but a relatively weak deshielding effect on ^{29}Si nuclei of Si^0 and Si^{III} centers: $Si_{20}(SiCl_3)_{12}Cl_8$: δ(^{29}Si, calcd) = –63.1 (Si^0), 53.9 (Si^I), 7.9 (Si^{III}); $[Cl@Si_{20}(SiCl_3)_{12}Cl_8]^-$ ([**1**]$^-$): δ(^{29}Si, calcd) = –59.9 (Si^0), 31.6 (Si^I), 13.3 (Si^{III}): Ponce-Vargas, M.; Muñoz-Castro, A. Stabilizing Role of Halide Ions in Endohedral [20]Silafulleranes: Insights from DFT Calculations toward Silicon Nanocages. *J. Phys. Chem. C* **2018**, *122*, 12551–12558. https://doi.org/10.1021/acs.jpcc.8b03360. For the results of our calculations on the derivatives of [**1**]$^-$–[**4**]$^-$ without endohedral Cl^- ions, see Table S5.

(72) Adamo, C.; Barone, V. Toward reliable density functional methods without adjustable parameters: The PBE0 model. *J. Chem. Phys.* **1999**, *110*, 6158–6170. https://doi.org/10.1063/1.478522.

(73) Klamt, A.; Schüürmann, G. COSMO: a new approach to dielectric screening in solvents with explicit expressions for the screening energy and its gradient. *J. Chem. Soc., Perkin Trans. 2* **1993**, *5*, 799–805. https://doi.org/10.1039/P29930000799

(74) van Lenthe, E.; Baerends, E. J.; Snijders, J. G. Relativistic total energy using regular approximations. *J. Chem. Phys.* **1994**, *101*, 9783–9792. https://doi.org/10.1063/1.467943

(75) Mo, Y.; Zhang, Y.; Gao, J. A Simple Electrostatic Model for Trisilylamine: Theoretical Examinations of the n→σ* Negative Hyperconjugation, $p_\pi \rightarrow d_\pi$ Bonding, and Stereoelectronic Interaction. *J. Am. Chem. Soc.* **1999**, *121*, 5737–5742. https://doi.org/10.1021/ja9904742.

(76) Rüger, R.; Franchini, M.; Trnka, T.; Yakovlev, A.; van Lente, E.; Philipsen, P.; van Vuren, T.; Klumpers, B.; Soini, T. ADF 2022.1, SCM, Theoretical Chemistry, Vrije Universiteit, Amsterdam, The Netherlands, http://www.scm.com. 2022 (accessed 2023-04-21).

(77) Schreckenbach, G.; Ziegler, T. Calculation of NMR Shielding Tensors Using Gauge-Including Atomic Orbitals and Modern Density Functional Theory. *J. Phys. Chem.* **1995**, *99*, 606–611. https://doi.org/10.1021/j100002a024

(78) Pye, C. C.; Ziegler, T.; van Lenthe, E.; Louwen, J. N. An implementation of the conductor-like screening model of solvation within the Amsterdam density functional package – Part II. COSMO for real solvents. *Can. J. Chem.* **2009**, *87*, 790–797. https://doi.org/10.1139/V09-008

(79) van Lenthe, E.; Baerends, E. J. Optimized Slater-type basis sets for the elements 1–118. *J. Comput. Chem.* **2003**, *24*, 1142–1156. https://doi.org/10.1002/jcc.10255

(80) Lehmann, J. F.; Schrobilgen, G. J.; Christe, K. O.; Kornath, A.; Suontamo, R. J. X-ray Crystal Structures of $[XF_6][Sb_2F_{11}]$ (X = Cl, Br, I); ^{35,37}Cl, ^{79,81}Br, and ^{127}I NMR Studies and Electronic Structure Calculations of the XF_6^+ Cations. *Inorg. Chem.* **2004**, *43*, 6905–6921. https://doi.org/10.1021/ic040015o

(81) Jaszuński, M.; Mikkelsen, K. V.; Rizzo, A.; Witanowski, M. A Study of the Nitrogen NMR Spectra of Azoles and Their Solvent Dependence. *J. Phys. Chem. A* **2000**, *104*, 1466–1473. https://doi.org/10.1021/jp994204h

(82) Philips, A.; Marchenko, A.; Ducati, L. C.; Autschbach, J. Quadrupolar ^{14}N NMR Relaxation from Force-Field and Ab Initio Molecular Dynamics in Different Solvents. *J. Chem. Theory Comput.* **2019**, *15*, 509–519. https://doi.org/10.1021/acs.jctc.8b00807

(83) Deviations from 0 are due to artificial symmetry breaking inherent to the method applied.

(84) Marciniec, B. Catalysis by transition metal complexes of alkene silylation – recent progress and mechanistic implications. *Coord. Chem. Rev.* **2005**, *249*, 2374–2390. https://doi.org/10.1016/j.ccr.2005.02.025

(85) Troegel, D.; Stohrer, J. Recent advances and actual challenges in late transition metal catalyzed hydrosilylation of olefins from an industrial point of view. *Coord. Chem. Rev.* **2011**, *255*, 1440–1459. https://doi.org/10.1016/j.ccr.2010.12.025

(86) Tilley, T. D. The Coordination Polymerization of Silanes to Polysilanes by a "σ-Bond Metathesis" Mechanism. Implications for Linear Chain Growth. *Acc. Chem. Res.* **1993**, *26*, 22–29. https://doi.org/10.1021/ar00025a004

(87) Corey, J. Y. Dehydrocoupling of Hydrosilanes to Polysilanes and Silicon Oligomers: A 30 Year Overview. *Adv. Organomet. Chem.* **2004**, *51*, 1–52. https://doi.org/10.1016/S0065-3055(03)51001-2

(88) Bock, H.; Ensslin, W. Bond-Bond Interaction in Polysilanes. *Angew. Chem., Int. Ed. Engl.* **1971**, *10*, 404–405. https://doi.org/10.1002/anie.197104041

(89) Miller, R. D.; Michl, J. Polysilane High Polymers. *Chem. Rev.* **1989**, *89*, 1359–1410. https://doi.org/10.1021/cr00096a006

(90) Ishida, S.; Otsuka, K.; Toma, Y.; Kyushin, S. An Organosilicon Cluster with an Octasilacuneane Core: A Missing Silicon Cage Motif. *Angew. Chem., Int. Ed.* **2013**, *52*, 2507–2510. https://doi.org/10.1002/anie.201208506

(91) Jovanovic, M.; Michl, J. Alkanes versus Oligosilanes: Conformational Effects on σ-Electron Delocalization. *J. Am. Chem. Soc.* **2022**, *144*, 463–477. https://doi.org/10.1021/jacs.1c10616

Authors are required to submit a graphic entry for the Table of Contents (TOC) that, in conjunction with the manuscript title, should give the reader a representative idea of one of the following: A key structure, reaction, equation, concept, or theorem, etc., that is discussed in the manuscript. Consult the journal's Instructions for Authors for TOC graphic specifications.

Insert Table of Contents artwork here

TOC Graphic: